The Starting Transient in a Gas-Generator Hybrid Rocket Motor

Alexander Osherov and Benveniste Natan*

Faculty of Aerospace Engineering, Technion – Israel Institute of Technology, Haifa 32000 (Israel)

Der Anzündvorgang in einem Hybrid-Raketenmotor mit Gasgenerator

Es wird ein Modell zur Voraussage des Anzündvorganges in einem Hybrid-Raketenmotor mit Gasgenerator vorgestellt. Das Modell bezieht wichtige Auslegungsparameter mit ein, sowohl komplizierte Ladungskonfigurationen, diverse Randbedingungen, erosive Abbrandgeschwindigkeiten, als auch räumlich und zeitlich variierende thermodynamische Eigenschaften des festen Gasgenerators sowie der Gasströmung. Der ausgearbeitete numerische Code demonstriert für Modellfälle eine hohe Leistungsfähigkeit, zeitabhängige fluiddynamische Probleme zu lösen und erweist sich insbesondere für innenballistische Fragestellungen wie auch für Stabilitätsbetrachtungen als nützlich. Mehrere Fälle von Anzündvorgängen eines grossen Motors werden betrachtet und ''Worst Case''-Situationen erkannt.

Processus d'allumage d'un moteur de fusée hybride à générateur de gaz

On présente un modèle de prédiction du processus d'allumage dans un moteur de fusée hybride à générateur de gaz. Le modèle considère des paramètres de dimensionnement importants tels que des configurations de charges compliquées, diverses conditions aux limites, des vitesses de combustion érosives ainsi que des propriétés thermodynamiques variables dans l'espace et dans le temps du générateur de gaz et de l'écoulement gazeux. Le code numérique développé pour la modélisation est très performant pour résoudre des problèmes de dynamique des fluides liés au temps et s'avère utile, en particulier pour les questions de balistique intérieure ainsi que pour l'analyse de stabilité. Plusieurs cas d'allumage d'un moteur de grande taille sont considérés et des situations de type Worst Case" sont identifiées.

Summary

A model for the prediction of the starting transient in a gas-generator hybrid motor is presented. The model considers essential design parameters such as complex grain configuration, boundary conditions, erosive burning rate, as well as spatially and temporally variable thermodynamic properties of both condensed material and gas flow. The developed numerical code for the model solution demonstrates a strong capability for solving time-dependent fluid dynamics problems and can be particularly useful for internal ballistics considerations as well as for stability analysis. Several scenarios for starting transients of a large-size motor are considered and worst case events are identified.

1. Introduction

After the Titan and Challenger accidents, the hybrid motor concept was reconsidered especially for advanced launch vehicle application due to its safety characteristics. The hybrid motor combines the advantages of the solid rocket motor with those of the bipropellant liquid motor: high specific impulse, improved safety, low cost, wide-range control, clean exhaust products, and low sensitivity to fuel grain defects[1–3].

In general, two main types of hybrid motors suitable for use in space systems can be considered: the "classic" and the "gas-generator" type hybrid motors. Both concepts can achieve start-up, shutdown, and throttling.

In the classic hybrid motor a liquid oxidizer is injected into the forward end of an inert solid fuel grain port. Extensive research[4–6] demonstrated that the fuel regression rate and the mixture ratio are controlled by heat transfer processes, heterogeneous fuel decomposition reactions, fuel-oxidizer mixing and gas-phase combustion that occurs in the turbulent boundary layer diffusion flame near the solid fuel surface. Simple theories based upon heat-transfer limited burning rate, can explain the experimentally observed fact that at low mass flow rates and high pressures, the regression rate is proportional to the oxidizer flux to the nth power[4,5], ($\dot{r} \propto G^n$) where $n = 0.6 - 0.8$.

A major problem in the classic hybrid motor is that the injector cannot distribute the oxidizer properly throughout the port that changes size and shape along the motor axis during operation. This results in excessive fuel residues remaining as slivers and it is difficult to utilize more then 95–97% of the fuel[2,7,8]. Hence, the design needs an afterburner chamber, which provides the desired mixing to improve combustion efficiency[7]. Moreover, since combustion occurs mainly within the boundary layer where the mixing of the fuel with the oxidizer is not adequate, the resulting fuel regression rate is low. To overcome this problem the surface area can be increased using multi-port grains. In such case, the thin webs must be supported by an internal structure to prevent collapse during flight, a complicated task because of the mechanical and manufacturing problems[2,6,8,9].

In addition, in the classic hybrid motor, thrust throttling causes mixture ratio and specific impulse variations and losses during operation. In principle, a secondary oxidizer injection may be added to the afterburner region increasing the gas temperature, but significant injector technology issues and system complexities arise.

In the gas-generator type hybrid motor, a solid propellant serves as the source of a fuel-rich gas at temperatures below 1300 K (gas generator), which is injected into the main (thrust) combustion chamber, where oxidizer is introduced

* Corresponding author; e-mail: aerbeny@aerodyne.technion.ac.il

 0721-3115/00/0511–0260 $17.50+.50/0

to complete the chemical reaction and utilize the energy potential (Figure 1).

The gas-generator propellants exhibit more marginal combustion characteristics than conventional solid propellants because of their oxidizer deficiency, their ignition is more difficult, but they can produce fuel gases at a significantly higher rate in comparison to the classic hybrid motor.

Several studies dealt with the basic similarities and differences between the two hybrid motor concepts[7,8]. Compared to the gas-generator type, the classic hybrid motor operates at high temperatures (about 2700 K) and high pressures that enhance the requirements for case insulation, sealing, and materials. In addition, since the volume required for the oxidizer injection and the multiple ports is significantly larger than the single port and thrust combustion chamber volume of the gas-generator type motor, the motor case weight should be bigger, too. Yet, according to an accelerating rate calorimeter (ARC) estimation[3], the classic hybrid motor is 0.5%−2.5% lighter than the equivalent gas-generator type hybrid motor. As regards cost, in the same report it is claimed that the lowest life-cycle cost was obtained by a turbopump-fed gas-generator type with HTPB and LOX, while a classic hybrid motor with pressure-fed H_2O_2 had the highest.

In contrast to the classic hybrid motor, flow control independent of thrust control is possible. During normal operation, the fuel-rich gas flow through the injector is subsonic allowing pressure changes in the thrust chamber to be transmitted to the gas generator. Changes in the injector geometry affect the pressure drop along the injector and since the propellant burning rate is pressure sensitive, flow rate control can be achieved by varying the injector inlet cross-section area. In general, the specific geometric and structural constraints make the starting transient of a hybrid motor a difficult and complex process.

For guidance and control purposes detailed knowledge of thrust during the ignition transient and the initial phase of motor operation is needed. Hence, high accuracy in the prediction and control of the ignition transient is required especially in large motors. In addition, both the gas-generator pressure and the rate of pressurization are of prime concern to designers in order to avoid peak pressures, which are much higher than the desired equilibrium pressure. In the opposite case, if the heat transfer rate is low and the ignited grain surface area is small, the flame cannot be spread adequately within a short period.

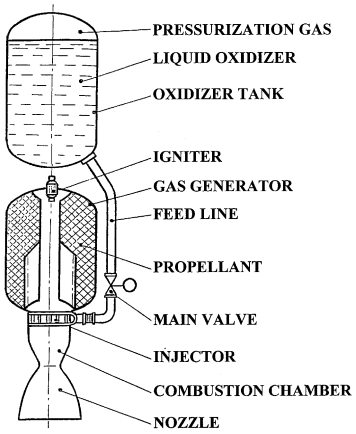

Figure 1. Configuration of a gas-generator hybrid rocket motor.

Several analytical, one-dimensional models were developed to predict the transient phenomena in the flowfield of solid and hybrid motors during ignition[10−13]. Johnston[14] conducted a simulation of the ignition process of the Titan and Space Shuttle solid motors, in which a star cross-section configuration propellant was considered. He used axisymmetric geometry for the flowfield, one-dimensional approach for the convective and radiative heat transfer to the propellant surface, and the ignition criterion was based on the surface temperature. Mathematical models of hybrid motor history during the early phases of operation supported by corresponding experiments were developed by Parker *et al*.[15]. A comparison between various analytical methods for the classic hybrid motor ignition calculation was published by Karabeyoglu *et al*.[16]. A numerical solution by Peretz *et al*.[12,13] exhibited a satisfactory agreement with experimental data. A comprehensive literature survey of the ignition transient in solid rockets was conducted by Kumar and Kuo[17].

The typical design and analysis goals for a successful ignition are: (a) provide reliable and stable ignition; (b) reduce the overpressure that sometimes accompanies ignition; (c) predict how a design modification will alter performance; (d) avoid narrow margins giants hang-fire; (e) provide a basis for defining and achieving the design and development goals with a minimum of expensive motor tests; (f) reduce motor-to-motor variations in the starting transients of clustered motors; (g) reduce the cost associated with experimental trials.

The prediction of the motor ignition transient depends on the understanding of the complex interactions between particular fundamental processes that take place: the igniter gas flow, convective heat transfer, flame spreading, the developing flowfield, erosive burning, starting of the liquid oxidizer feed system and the pressure-time history of the main (thrust) combustion chamber.

The objective of the present investigation is to develop a physical model, formulate it mathematically and produce a numerical algorithm for the prediction of the starting transient in a gas-generator hybrid motor.

2. Description of the Physical Model

The starting process in gas-generator hybrid motors can be described as follows:

At $t = 0$ the igniter at the head-end of the gas generator is initiated and dumps its high temperature combustion products into the gas-generator cavity through a sonic nozzle. In general, a cartridge-type, grain-mounted igniter with an environmental seal (diaphragm) or plug is used. To enhance ignition, long slots in the fuel-rich grain are overcast

by a solid propellant of high burning rate[3] that allows the oxidizer-fuel mixture to reach the required level in the combustion chamber after the starter grain is exhausted. Large gas generators are usually started by a pyrogenic igniter, which is basically a solid propellant motor operating for a short, finite time providing a given mass flow rate versus time. The incoming igniter gases generate a pressure wave, which propagates along the gas-generator port and is characterized by a front with steep pressure, velocity, and temperature gradients. The length of the solid reactant bed is gradually exposed to the flow behind the front of the hot gas. The gas-generator pressure is above the extinguishing limits of the propellant during a short time after igniter firing.

The first phase of the ignition corresponds to the induction period (ignition lag) required for propellant decomposition and gasification because of the finite thermal relaxation times of the solid reactants. This phase ends with the appearance of a flame on the propellant surface near the forward end. The second phase corresponds to the time period needed for flame spreading over the exposed surface of the propellant grain. The motion of the high temperature combustion products implies friction and heat transfer to the solid propellant surface causing increase of its temperature followed by degradation and vaporization. Once started, the flame spreading is accelerated towards the afterburner end by the increased heat flux due to the rapidly increasing mass flow originating from the already ignited propellant surface. Significant pressure and temperature drops as well as a velocity increase are established along the port. The products generated by the gas-generator discharge through its afterburner end injector. The third phase corresponds to gas-generator pressurization period (development of the flowfield in the gas generator), following the completion of flame spreading.

The oxidizer feeding system consists of the liquid oxidizer (typically cryogenic oxygen) tank that operates under high pressure, pipeline, main valve, manifold and injector. At some chosen moment $t = \tau_{v1}$ the main valve is opened to the first stage level. Oxidizer begins to fill the manifold and injector cavities and then is discharged through the injector into the combustion chamber. The pressure transient in the oxidizer pipeline accompanies this operation. Due to the pressure drop between the feed-line and the combustion chamber, the liquid oxidizer is dispersed, mixes with hot gaseous fuel from the gas generator and after a certain induction period (time delay) τ_c, it burns while the combustion chamber pressure is rising progressively. When the valve is opened to the main stage level at $t = \tau_{v2}$, the oxidizer mass flow rate and consequently the combustion chamber pressure abruptly increase toward quasi-steady operating conditions.

3. Analytical Model

The present analytical model deals with the ignition transient in the gas-generator type hybrid motor. The model considers four major areas:

A. Gas generator: One-dimensional development of the flowfield in the gas-generator port with time that considers mass, momentum and energy conservation equations for the combustion products flow, initial and boundary conditions for the gas flow at the head and afterburner end of the grain. The gas is assumed to be perfect. The propellant combustion product composition and thermodynamic properties (molecular weight, specific heat and flame temperature) are calculated at every point as functions of the given propellant composition and the local instant pressure. The port flow is assumed to be turbulent and an empirical correlation for the convective heat-transfer coefficient is used. The grain surface heat-up equation is coupled to an ignition criterion for the propellant. The burning rate of the solid propellant is calculated under erosive burning conditions.

B. Igniter: The mass conservation equation of the igniter gas with distinct thermodynamic properties is considered.

C. Oxidizer feed system: Mass and momentum conservation equations of an ideal compressible liquid flow within the pipeline are considered. The oxidizer manifold void cavity filling is taken into account. The gas velocity at the entrance to the injector is calculated for either choked or unchoked flow. The oxidizer main valve opens compulsory and the effective orifice area time-history is considered.

D. Combustion chamber: Mixing of the gas-generator flow with the oxidizer and consequent burning takes place in the combustion chamber. The mass and energy conservation equations of the combustion products are considered. The thermodynamic properties of the combustion chamber products are calculated assuming chemical equilibrium at the local instant pressure.

3.1 Core Flow Governing Equations

The gas-generator flowfield is considered as a region of predominant axial flow and wave motion[3]. It is described by a set of governing equations for mass, momentum, and energy conservation that are coupled with the ignition and flame spreading event and with the axial variation of mass addition. The one-dimensional assumption is a better approximation to the real situation. The flow properties depend upon the grain configuration and in the present case the geometry described in Figure 2 is adopted.

Mass conservation:

$$\frac{\partial(\rho A)}{\partial t} + \frac{\partial(\rho u A)}{\partial x} = \dot{r}_e \rho_p S \tag{1}$$

Neglecting viscous forces in the axial direction, the momentum conservation equation is described by:

$$\frac{\partial(\rho u A)}{\partial t} + \frac{\partial\left(\rho u^2 A\right)}{\partial x} + A\frac{\partial p}{\partial x} + \frac{1}{8} C_R \rho u^2 S = 0 \tag{2}$$

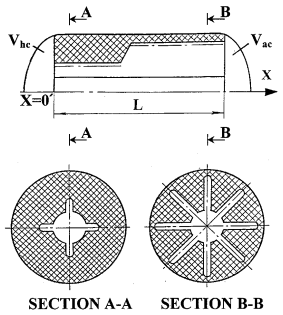

Figure 2. Typical configuration of a gas-generator propellant grain.

For the ignited part of the surface, the coefficient of resistance C_R is zero due to blowing, while for the non-ignited surface, C_R is given by:

$$C_R = 0.0032 + 0.22Re^{-0.24} \tag{3}$$

Neglecting (a) viscous dissipation and rate of work done by internal viscous forces and (b) molecular axial heat conduction, the energy conservation equation is described by:

$$\frac{\partial(\rho eA)}{\partial t} + \frac{\partial(\rho euA)}{\partial x} + \frac{\partial(upA)}{\partial x} = c_p T_f \rho_p \dot{r}_e S \tag{4}$$

The stagnation energy, e, is given by:

$$e = c_v T + \tfrac{1}{2}u^2 \tag{5}$$

Perfect gas assumption:

$$p = \rho RT \tag{6}$$

The grain geometry is assumed to be constant in time. During the starting transient, the port area change due to surface regression is negligible. In general, there is a rapid increase in the pressure load on the propellant during ignition and grain deformation can alter the internal geometry (a coupled flow-structure interaction). Hence, the constant grain geometry assumption is valid only if the propellant deformation is small.

3.2 Boundary Conditions

The implicit numerical method adopted in the present investigation to solve the system of the hyperbolic equations, Eqs. (1), (2) and (4), requires six boundary conditions. There are only three physical conditions for this purpose. To obtain the other three missing boundary conditions, the method described by Kuo *et al.*[10,11] and Peretz *et al.*[12,13] is used, according to which, extraneous equations obtained by the method of characteristics are defined. This method is based on the following approach. Since the three governing partial differential equations are hyperbolic, all three eigenvalues of the characteristic equation are real and are given by u (particle-path line) $dx/dt = u - a$ (left-running Mach line), and $dx/dt = u + a$ (right-running Mach line). These equations may be rewritten in their characteristic form, in which each equation displays the derivatives in the direction of one of the characteristic lines only. At the boundaries, the characteristic form equations (which are treated as ordinary differential equations) are equivalent to the compatibility conditions.

3.2.1 Upstream Boundary

The values of $u(t)$, $T(t)$, and $p(t)$ at $x = 0$ must be defined. Two equations that provide evaluation of these properties are valid along the upstream (left) boundary and they are obtained from mass and energy conservation at the head-end cavity:

$$\dot{m}_{hc} = \dot{m}_{ign} - [\rho uA]_{x=0} \tag{7}$$

$$c_v V_{hc}\left[\frac{d(T\cdot\rho)}{dt}\right]_{x=0} = \dot{m}_{ign}c_{p,ign}T_{ign} - \left[c_p T\cdot\rho uA\right]_{x=0} \tag{8}$$

Equations (7) and (8) yield stagnation values for gas temperature, T, and pressure, p, within the head-end cavity.

The third left boundary condition is given by the extraneous equation (Kuo *et al.*[11]), which is valid along the "left-directed", λ_I, characteristic line:

$$\left.\frac{du}{dt}\right|_{\lambda_I} = -a_1\left.\frac{dp}{dt}\right|_{\lambda_I} - D_1 \tag{9}$$

3.2.2 Downstream Boundary

Three equations are necessary to evaluate $u(t)$, $T(t)$, and $p(t)$ at $x = L$. There is only one physical boundary condition, which may be formulated by using the energy conservation equation for the aft-end cavity:

$$\left.\frac{dp}{dt}\right|_{x=L} = p_{ac}\left(u_L - u_{inj}\frac{C_D A_{inj}}{A_L}\right)\frac{\gamma A_L}{V_{ac}} \tag{10}$$

The isentropic flow velocity of the gas-generator products through the injector orifices depends on the pressure ratio p_L/p_c. If $p_L/p_c < \left(\frac{\gamma+1}{2}\right)^{\gamma/(\gamma-1)}$ the flow is subsonic and the velocity is given by:

$$u_{inj} = \left\{2\frac{\gamma}{\gamma-1}RT\left[\left(\frac{p_c}{p_L}\right)^{2/\gamma} - \left(\frac{p_c}{p_L}\right)^{(\gamma+1)/\gamma}\right]\right\}^{1/2} \tag{11}$$

If the flow is choked the velocity is given by:

$$u_{inj,ch} = \sqrt{\gamma RT\left(\frac{\gamma+1}{2}\right)^{-(\gamma+1/\gamma-1)}} \tag{12}$$

In addition, it is assumed that $p_L = p_{ac}$.

The second and third boundary conditions are obtained by extraneous equations valid along the "right-directed", λ_{II}, and the "particle path-directed", λ_{III}, characteristic lines can be written respectively:

$$\left.\frac{du}{dt}\right|_{\lambda_{II}} = -a_2\left.\frac{dp}{dt}\right|_{\lambda_{II}} - D_2 \tag{13}$$

$$\left.\frac{dT}{dt}\right|_{\lambda_{III}} = -a_3 \left.\frac{dp}{dt}\right|_{\lambda_{III}} - D_3 \tag{14}$$

3.3 Igniter Gas Flow

The igniter gas flow continuity equation is described by:

$$\frac{\partial(\rho_{ign}A)}{\partial t} + \frac{\partial(\rho_{ign}uA)}{\partial x} = 0 \tag{15}$$

Equation (15) is reduced to:

$$\frac{\partial \rho_{ign}}{\partial t} + u\frac{\partial \rho_{ign}}{\partial x} = -\rho_{ign}\left(\frac{\partial u}{\partial x} + \frac{u}{A}\frac{dA}{dx}\right) \tag{16}$$

The upstream boundary condition ($x = 0$) is given by:

$$\rho_{ign}\Big|_{x=0} = Y_{ign}\left.\frac{p}{RT}\right|_{x=0} \tag{17}$$

3.4 Gas-Generator Products Composition

The thermodynamic properties of the gas-generator products (molecular weight, specific heat capacity and temperature) at every point are calculated assuming chemical equilibrium. For the calculation PEP code[18] is utilized and the input is the propellant composition and the local instant pressure.

The flow contains particulate matter and the thermodynamic properties are calculated for a gas-particle mixture. The total density of the core flow products composition:

$$\rho = \rho_{p,g} + \rho_{p,s} + \rho_{ign} \tag{18}$$

The content of the gaseous propellant products depends on the propellant composition and is assumed to be constant.

$$K_g = \frac{m_{p,g}}{m_{p,g} + m_{p,s}} = \frac{\rho_{p,g}}{\rho_{p,g} + \rho_{p,s}} = \frac{Y_{p,g}}{Y_{p,g} + Y_{p,s}} \tag{19}$$

Thus the gaseous propellant product mass fraction in the mixture is given by:

$$Y_{p,g} = K_g(1 - Y_{ign}) \tag{20}$$

The overall gas constant is derived from the relation:

$$R = Y_{ign}R_{ign} + K_g \cdot (1 - Y_{ign})R_{p,g} \tag{21}$$

3.5 Propellant Surface Temperature

The ignition criterion is that a point on the propellant surface ignites when it attains a critical ignition temperature. Thus, the process of flame spreading along the grain surface can be described by the model of successive heating and ignition.

The analysis assumes that the propellant internal thermal resistance is much higher than the surface one, and the grain is cured at a bulk temperature, T_o. The thermal wave penetration depth (defined from the grain surface inward) due to heat transfer is expected to be of the order of $O\langle k_p(T_s - T_o)/h(T - T_s)\rangle \approx 0.1\,\text{mm}$, hence, it is much smaller then a typical grain radius. The associated time scale is also very short and is expected to be less then 0.01 s.

Taking into consideration these characteristics, the propellant temperature at the $z = 0$ boundary, $T_s = T_p(t, 0)$, can be calculated. In reality, the grain temperature tends asymptotically to T_o. In the present investigation it is assumed that the temperature profile of the heat-up layer at the grain surface, $T_p(t, z)$, can be approximated by a third-order polynomial described by:

$$T_p(t, z) - T_o = \zeta_0(t) + \zeta_1(t) \cdot z + \zeta_2(t) \cdot z^2 + \zeta_3(t) \cdot z^3 \tag{22}$$

The time-dependent coefficients, ζ_0, ζ_1, ζ_2, ζ_3, are evaluated by taking into account the following boundary conditions:

$$\begin{aligned} &T_p\big|_{z=z_o} = T_o, \quad \left.\frac{\partial T_p}{\partial z}\right|_{z=z_o} = 0, \quad \left.\frac{\partial^2 T_p}{\partial z^2}\right|_{z=z_o} = 0, \\ &\left.\frac{\partial T_p}{\partial z}\right|_{z=0} = -\frac{1}{k_p}q(t, x)\big|_{z=0} \end{aligned} \tag{23}$$

The effective thermal penetration distance, z_o, is calculated from heat transfer considerations.

The calculations yield:

$$T_p(t, z) - T_o = \frac{q}{3k_p z_o^2}(z_o - z)^3 \tag{24}$$

Therefore, the effective thermal penetration distance for a flat plate is given by:

$$z_o = \frac{3k_p}{q(t, x)}(T_s - T_o) \tag{25}$$

The grain surface is assumed to be heated by convection and radiation. The influence of the longitudinal heat conduction at the grain surface even near the flame front was found to be negligible[19]. It should be noted that radiation from both gas and fine powdery soot (carbon particles smaller than 0.1 μm diameter size) can be an important contributor to the heat flux especially in non-metallized fuels[20]. In the present case, the combustion products may contain clouds of finely dispersed solid matter. Such particles can be very effective blackbody emitters. Especially for gas generators, the particle radiation is rather significant because of the high molecular and particle number densities. Radiation is especially important inside the propellant slots, where the gas velocity is low and the effect of convection is diminished. Since it is difficult to estimate the combined effect of gas emissivity and transmittance and surface absorptivity, an empirical radiative heat transfer correction factor equal to 0.25 is assumed to account for the transfer coefficients[14]. Gas emissivity is assumed to increase proportionally to T_g^4 and the combustion chamber pressure, whereas the particle radiation is proportional to T_{part}^4.

At any point, x, along the grain port, the total heat flux from the gas to the propellant surface is described by:

$$q(t, x) = h(T - T_s) + \varepsilon\sigma\left(T^4 - T_s^4\right) \tag{26}$$

Under the above assumptions, the Fourier equation for a flat plate surface heating may be written as an ordinary differential equation:

$$\frac{dT_s}{dt} = \theta_1 \frac{dT}{dt} + \theta_2 \frac{dh}{dt} + \theta_3 \tag{27}$$

The coefficients, θ_k, are functions of T, T_s, h, k_p and α_p.

The port flow is highly turbulent and the Dittus-Boetler empirical correlation for the convective heat-transfer is adopted (Peretz[19]). The coefficient for no-blowing heat transfer from the flow to the surface is given by:

$$h = 0.023 c_p \mu \, Pr^{-0.6} Re_x^{0.8}/x \tag{28}$$

where the local flow Reynolds number is defined by:

$$\mathrm{Re}_x = \frac{\rho u x}{\mu} \tag{29}$$

3.6 Propellant Burning Rate

In the early studies on the solid propellant ignition problem a quasi-steady burning rate law was assumed, however, experiments showed that this assumption was not adequate[12]. The literature treating the transient regression rates is deficient. In the present case, a modified Lenoir-Robillard[12,21] erosive burning model is used because of the good agreement between its predictions and experimental data.

For the erosive burning rate the following empirical correlation is used:

$$\dot{r}_e(x) = \dot{r}_b + h \cdot k_b \cdot \exp\left(-\beta \cdot \dot{r}_b \cdot \rho_p / G\right) \tag{30}$$

The gas-generator propellant cannot burn below a certain extinguishing pressure limit p^*, therefore, a prediction that considers threshold phenomena is important for a proper starting evaluation. In this case the normal unperturbed burning rate, $\dot{r}_b$, is given by:

$$\dot{r}_b = a_b (p - p^*)^n \cdot u(p - p^*) \tag{31}$$

where u is Heaviside function.

The extinguishing pressure limit p^*, k_b, and β are empirical constants of the propellant.

3.7 Oxidizer Feed System: Pipe-Line and Control Valve

The flow within a long pipe from the tank containing an ideal compressible liquid oxidizer (LOX for example) is described by a set of two governing equations for mass and momentum conservation:

$$\frac{\partial p}{\partial t} + a^2 \rho_{ox} \frac{\partial v}{\partial y} = 0 \tag{32}$$

$$\frac{\partial v}{\partial t} + \frac{1}{\rho_{ox}} \frac{\partial p}{\partial y} = 0 \tag{33}$$

Two boundary conditions are adopted. The pipe on the left side ($y = 0$) is directly connected to a large volume LOX tank, which from the acoustic point of view is considered as an "open end":

$$p(0, t) = p_{\text{tank}} \tag{34}$$

On the right side, $y = \ell$, the pipe is connected to the main control valve whose effective orifice area varies compulsory in time. In the time period from the beginning of the valve opening and before the manifold cavity volume, V_m, filling, the hydraulic resistance area, $(C_D \cdot A)$, is defined by the valve orifice area only. After the manifold and the oxidizer injector cavities are completely filled, the effective hydraulic resistance area is defined as a series of hydraulic resistance areas. Therefore, the mass flow rate is described by:

$$\dot{m}_v = (C_D \cdot A)_{eff} \cdot \sqrt{2\rho_{ox}(p_\ell - p_c)} \tag{35}$$

The effective hydraulic resistance area, $(C_D \cdot A)_{eff}$, is given by:

$$(C_D \cdot A)_{eff} = (C_D \cdot A)_v \quad \text{if} \quad V_m - V_{m,v} > 0 \tag{36}$$

where $V_{m,v}$ is the volume of the liquid that passed through the valve.

After the manifold and oxidizer injector cavities are completely filled the effective hydraulic resistance area is described by:

$$(C_D \cdot A)_{eff} = \left[(C_D \cdot A)_{inj}^{-2} + (C_D \cdot A)_v^{-2}\right]^{-0.5} \tag{37}$$

By introducing the notation:

$$\alpha(t) = \left[\frac{A_{pl}}{(C_D \cdot A)_{eff}}\right]^2 \tag{38}$$

Equation (35) may be rewritten in the form:

$$\frac{1}{2}\rho_{ox} \cdot v_\ell^2(t) \cdot \alpha(t) = p_\ell(t) - p_c(t) \tag{39}$$

3.8 Combustion Chamber

The mass conservation equation of the combustion chamber gaseous products is given by:

$$\frac{dm_c}{dt} = \dot{m}_{inj} - \dot{m}_{th} + \dot{m}_{ox,\langle t-\tau\rangle} \tag{40}$$

A time delay, τ, is assumed due to the processes of heating, vaporization and mixing of the liquid oxidizer (cryogenic LOX).

The instant mixture ratio, calculated by taking into account the time lag and the mass fraction of the propellant combustion products in the gas-generator products, is described by:

$$MR = \frac{\dot{m}_{ox,\langle t-\tau\rangle}}{\left[\dot{m} \cdot (1 - Y_{ign})\right]_{inj}} \tag{41}$$

The thermodynamic properties of the combustion chamber products are calculated assuming chemical equilibrium. For this purpose, the PEP thermochemical code[18] is utilized

with an input of the mixture ratio and the combustion chamber pressure.

The energy conservation equation is expressed by:

$$\frac{dT_c}{dt} = -\frac{T_c}{m_c}\left[\dot{m}_{inj} + (\gamma - 1)\dot{m}_{th} + \dot{m}_{ox,\langle t-\tau\rangle}\right] + \frac{\left[c_p T \dot{m} Y_{ign}\right]_{inj} + h_c\left\{\left[\dot{m}(1 - Y_{ign})\right]_{inj} + \dot{m}_{ox,\langle t-\tau\rangle}\right\}}{m_c c_{v,c}} \tag{42}$$

The combustion chamber enthalpy, h_c, includes the heat release from the combustion of the propellant products with the oxidizer.

4. Numerical Solution

The numerical scheme adopted in the present investigation is based on central-differences in space and generalized implicit differences in time. The non-linear governing equations for the variable properties, u, T and p, are written in the following form:

$$\frac{\partial \phi_i}{\partial t} = \sum_{j=1}^{3} F_{ij}\frac{\partial \phi_j}{\partial x} + Q_i \qquad (\phi_1 = u, \phi_2 = T, \phi_3 = p) \tag{43}$$

To allow the use of regular matrix inversion algorithms, a quasi-linearization procedure is utilized for the non-linear terms at each time step, Δt. The non-homogeneous terms, $Q_{i,n}$, at any point, n, in space, are linearized applying the following form in a predictor-corrector sequence:

$$Q_{i,n}^{j+1} = Q_{i,n}^{j} + \Delta Q_{i,n}^{j} \tag{44}$$

$$\Delta Q_{i,n}^{j} = \sum_{k=1}^{3} \frac{\partial Q_{i,n}^{j}}{\partial \phi_k} \cdot \Delta \phi_k \tag{45}$$

The numerical method used in the present investigation was also used by Kuo *et al.*[10,11] and Peretz *et al.*[12,13], and provides good stability and fast convergence.

The time-step varied from 10^{-4} s to 10^{-3} s for an $N = 50$ steps in space. Runs with 10 and 100 space-steps were conducted to verify numerical accuracy. There were insignificant differences between the 50 and 100 space-steps runs and the numerical error was estimated as 0.6%.

5. Results and Discussion

To demonstrate the influence of various design parameters on the successful starting of a hybrid motor towards its nominal operation regime, a hypothetical, yet realistic, large size ($5 \cdot 10^6$ N) gas-generator type hybrid motor is examined (Figure 1).

The gas-generator grain has a center-perforated configuration of a 10-m bore length with four/eight slots equally spaced around the circumference. It is assumed that void cavities are included within the gas-generator chamber configuration, as it is usually designed in solid propellant motors (Figure 2).

The grain length was chosen to provide a combustion chamber nominal operating pressure of 10 MPa. The gas-generator pressure level is only slightly higher than the combustion chamber pressure.

The gas-generator propellant composition is 78% solid binder, hydroxy-terminated polybutadiene (HTPB), filled with 22% solid ammonium perchlorate (AP). Such a fuel-rich propellant tends to exhibit low regression rates and would not burn below 1–3 MPa. In the combustion chamber, liquid oxygen (LOX) is used as oxidizer. Several pyrogenic igniters with different mass flow rates and time durations are used.

The various properties and baseline data of the motor appear in Table 1. Four different starting transient scenarios of the hybrid motor were investigated:

(a) Completely successful starting towards nominal steady state regime;
(b) Unsuccessful starting accompanied by a fading away propellant combustion;
(c) Unstable starting accompanied by pressure oscillations in the combustion chamber;
(d) A disastrous case when the motor is destroyed.

Detailed results of a successful starting prediction are presented in Figures 3–7. The mass flow rates of the igniter gas, the oxidizer and total flow through the injector are shown in Figure 3a and the resulting combustion chamber pressure and temperature are presented in Figure 3b. At $t = 170$ ms, the igniter has completely burned out and almost all the propellant grain surface is already ignited. Pressure rises and at $t = 250$ ms a steady-state temperature of approximately 3500 K is reached. The changes of the various properties in time along the propellant grain are presented in 3-D diagrams in Figures 4–7 (respectively the specific mass flow rate of the propellant, pressure, temperature and velocity). It seems that propellant ignition takes place after some induction period (ignition lag) and that intense propellant burning begins after the gas-generator pressure exceeds the propellant ignition threshold level (which is 1.5 MPa). Simultaneously, the combustion chamber pressure increase due to the beginning of LOX discharge causes some depression of the mass flow rate of the gas-generator products through the injector, resulting, therefore in additional gas-generator pressure raising. As shown in Figure 7, the velocity at the aft-end of the grain is rather high and erosive burning cannot be neglected.

An unsuccessful starting transient scenario is shown in Figure 8. Due to the small igniter charge (Figure 8a), the gas-generator pressure (Figure 8b) does not reach the pressure level which corresponds to the propellant intense burning before the igniter is completely burned out and hence grain burning is fading away. When LOX begins to discharge, the combustion chamber pressure raises and quickly exceeds the gas-generator pressure value. Such situation is considered as a failure.

Table 1. Baseline Data

Motor Characteristics	
F	5 MN
c^*	1710 m/s
c_F	1.648
I_{sp} (*sea level*)	285 s
$\dot{m}_{total}$	1783 kg/s
$\dot{m}_{ox}$	1070 kg/s
MR	1.5
Initial Conditions	
R_o	287 J/kg K
c_{po}	1000 J/kg K
c_{vo}	717 J/kg K
T_o	300 K
p_o	1 bar
Igniter	
M_{ign}	22
c_{pign}	1925 J/kg K
c_{vign}	1690 J/kg K
T_{ign}	3300 K
k_{ign}	$0.073 + 2.9 \cdot 10^{-5} \cdot T_{ign}$ J/m s K
R_{ign}	378 J/kg K
Combustion Chamber	
A_{th}	0.35 m^2
V_c	0.5 m^3
τ_c	5 ms
Gas Generator	
L	10 m
V_{hc}	0.3 m^3
V_{ac}	0.5 m^3
ρ_p	1130 kg/m^3
K_g	0.7
T_p	1220 K
ε	0.7
σ	$0.567 \cdot 10^{-7}$ J/s m^2 K^4
k_p	$0.038 + 1.12 \cdot 10^{-3} \cdot T_o$ J/m s K
c_p	1380 J/kg K
α_{th}	$0.241 \cdot 10^{-6}$ m^2/s
T_{ig}	600 K
p^*	1.5 MPa
a_b	$3.18 \cdot 10^{-4}$ m/s Pa$^{0.3}$
β	105
n	0.3
k_b	13700 m^3 K/J
Oxidizer Feed System	
$(C_D A)_{inj}$	0.075 m^2
τ_{v1}	0 ms
$(C_D A)_{v1}$	0.002 m^2
τ_{v2}	250 ms
$(C_D A)_{v2}$	0.022 m^2
ρ_{ox}	1130 kg/m^3
ℓ	12.5 m
A_{pl}	0.05 m^2
V_m	0.05 m^3
T_{ox}	80 K
Δp_v	0.3 MPa
Δp_{pl}	0.4 MPa
Δp_m	0.3 MPa

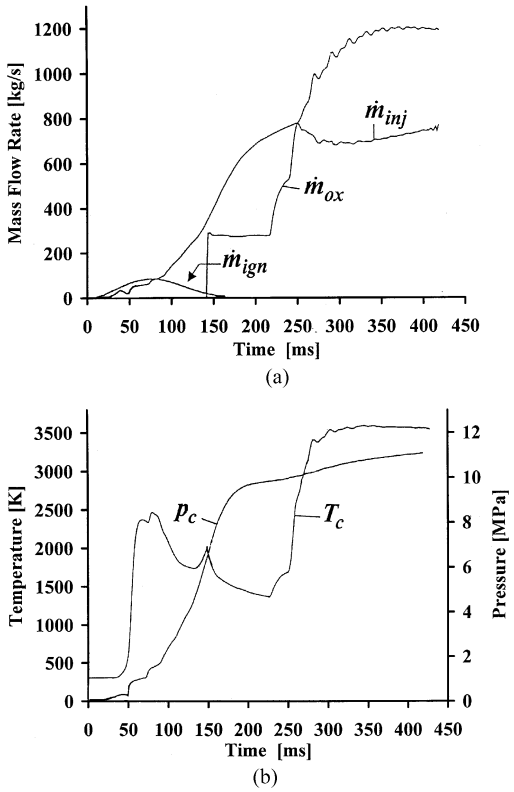

Figure 3. Successful starting transient. (a) Mass flow rates of oxidizer, igniter gas, injector gas, (b) combustion chamber temperature and pressure.

A peculiar case of an unstable starting transient is presented in Figure 9. During the main stage of the LOX valve operation, oscillations in the oxidizer flow occur (Figure 9a) that result in an oscillatory behavior in the combustion chamber pressure (Figure 9b) and consequent oscillations in the injector mass flow rate. Apparently, the main reason for this unacceptable event is the low pressure-drop ($p_{inj} - p_c$) at the injector.

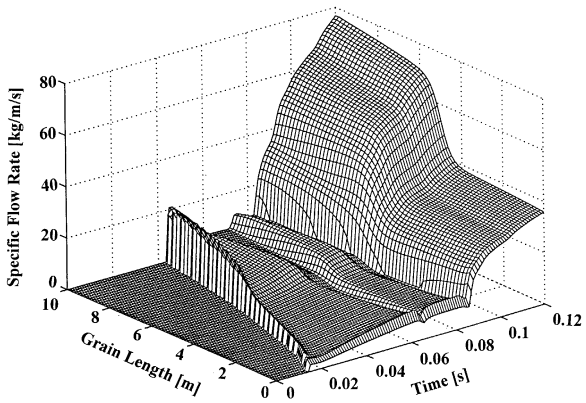

Figure 4. Successful starting transient. Gas-generator specific flow rate in space and time.

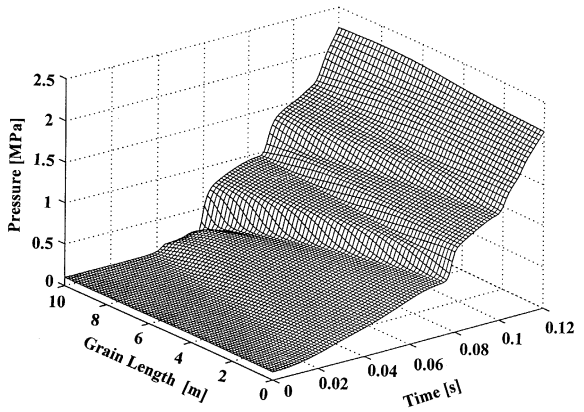

Figure 5. Successful starting transient. Gas-generator pressure growth in space and time.

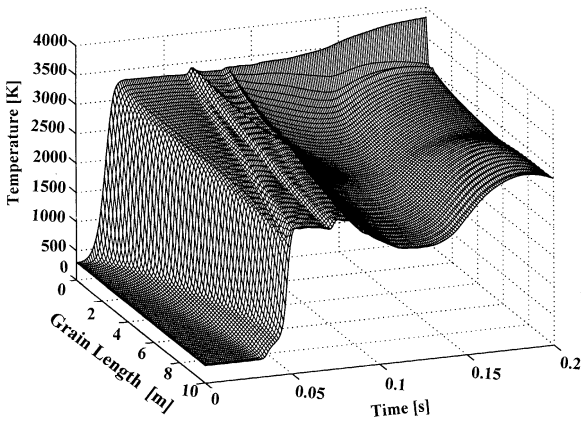

Figure 6. Successful starting transient. Gas-generator temperature growth in space and time.

In a most dangerous scenario, starting may be accompanied by destruction of the motor. Such a characteristic failure case is presented in Figure 10. At some moment ($t = 360$ ms) the total area of oxidizer injector orifices increases resulting in a very high LOX mass flow rate. The combustion chamber

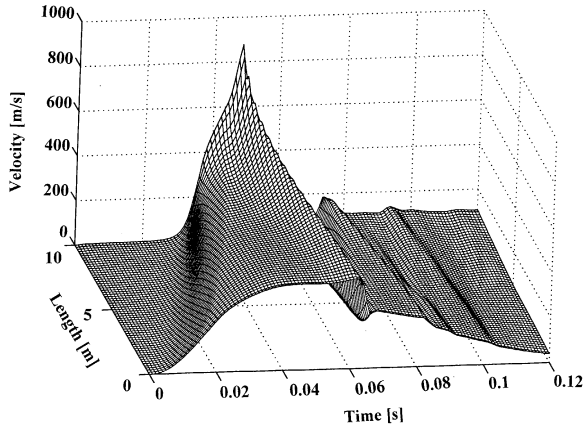

Figure 7. Successful starting transient. Gas-generator flow velocity in space and time.

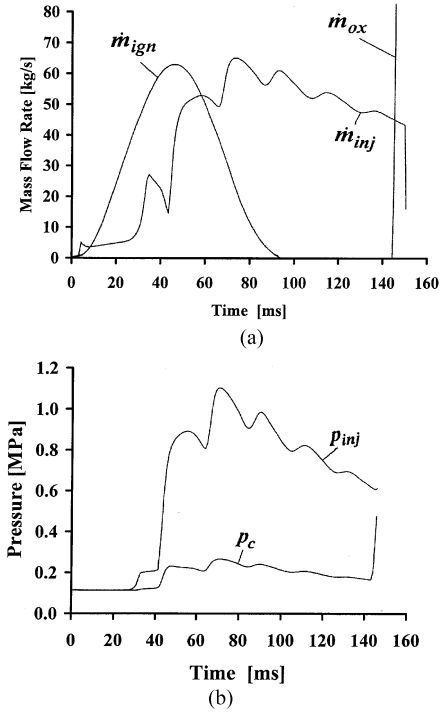

Figure 8. Unsuccessful starting transient. (a) Mass flow rates of oxidizer, igniter gas and injector gas, (b) gas generator and combustion chamber pressures.

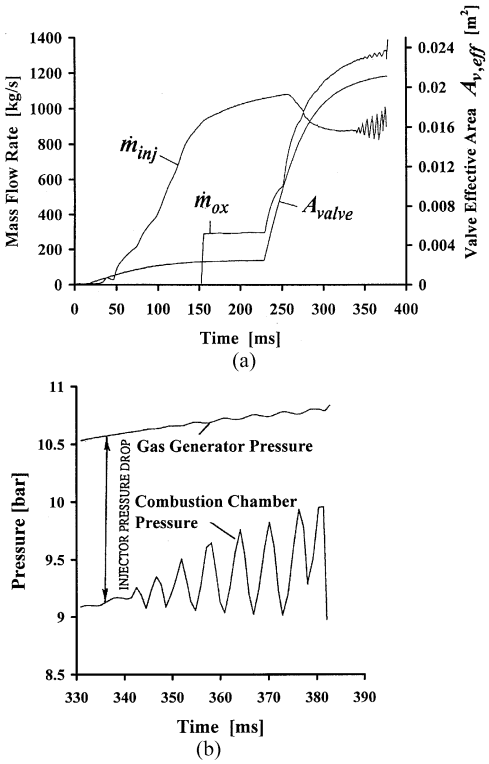

Figure 9. Unstable starting transient: (a) mass flow rates of oxidizer, injector gas and oxidizer valve effective area, (b) gas generator and combustion chamber pressures.

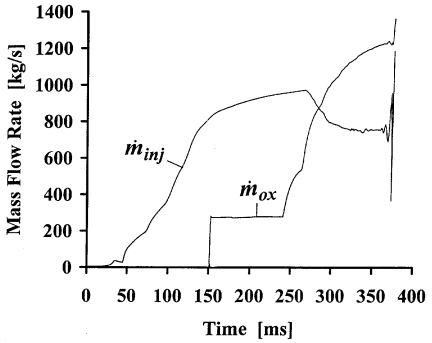

Figure 10. Disastrous starting transient. Mass flow rates of oxidizer and injector gas.

pressure increases to a very high level that is significantly higher than the nominal and leads to a catastrophic failure.

6. Conclusions

For the prediction of the starting transient in gas-generator type hybrid motor, a physical model, its mathematical formulation, and a numerical code were developed.

The model considers the essential hybrid motor design parameters, i.e., complex grain configuration, boundary conditions, erosive burning rate, as well as spatially and temporally variable thermodynamic properties of both condensed material and gas flow.

The numerical code demonstrates a very strong capability for solving time-dependent fluid dynamics problems and can be particularly useful for internal ballistics considerations as well as for stability analysis.

Several scenarios for starting transients of a large-size motor are considered and worst case events are identified. The results verify the importance of the present model for a successful starting design.

7. References

(1) D. Altman, "Hybrid Rocket Development History", *AIAA paper* 91–2515, 1991.
(2) K. R. Wagner and R. H. Schmucher, "Hybrid Rocket for Space Transportation–A Critical Assessment", *AIAA paper* 92–3305, 1992.
(3) "Hybrid Propulsion Technology Program Final Report", Contract NAS 8-37776, Report 90-26870 (1990), Atlantic Research Corporation, Gainsville, VA, USA.
(4) G. A. Marxman and M. Gilbert, "Turbulent Boundary Layer Combustion in the Hybrid Rocket", *9th Symposium (International) on Combustion*. The Combustion Institute, Pittsburgh, Pennsylvania, 1963, pp. 371–383.
(5) G. A. Marxman, "Boundary Layer Combustion in Propulsion", *11th Symposium (International) on Combustion*. The Combustion Institute, Pittsburgh, Pennsylvania, 1967, pp. 269–289.
(6) K. Ramohalli and J. Yi, "Hybrids Revisited", *AIAA paper* 90–1962, 1990.
(7) D. W. Culver and H. H. Mueggenburg, "Aft Mounted Gas/Liquid Injector Technology for Gas Generator Cycle Hybrid Rockets", *AIAA paper* 91–2518, 1991.
(8) D. W. Culver, "Comparison of Forward and Aft Injected Hybrid Rocket Boosters", *AIAA paper* 91–2586, 1991.
(9) B. Greiner and R. A. Frederick Jr., "Results of Labscale Hybrid Rocket Motor Investigation", *AIAA paper* 92–3301, 1992.
(10) K. K. Kuo, R. Vichnevetsky, and M. Summerfield, "Generation of an Accelerated Flame Front in a Porous Propellant", *AIAA paper* 71–210, 1971.
(11) K. K. Kuo, R. Vichnevetsky, and M. Summerfield, "Theory of Flame Front Propagation in Porous Propellant Charges under Confinement", *AIAA J.*, *11* (4), 444–451 (1973).
(12) A. Peretz, K. K. Kuo, L. H. Caveny, and M. Summerfield, "Starting Transient of Solid Propellant Rocket Motors with High Internal Gas Velocities", *AIAA J.*, *11* (12), 1719–1727 (1973).
(13) A. Peretz, "*The Starting Transient of Solid Propellant Rocket Motors with High Internal Gas Velocities*", Ph.D. Thesis (1973), AMS Dept., Princeton University, Princeton, NJ.
(14) W. A. Johnston, "Solid Rocket Motor Internal Flow During Ignition", *J. Propul. Power*, *11* (3), 489–496 (1995).
(15) K. H. Parker, W. J. Most, and M. Summerfield, "The Ignition Transient in Solid Propellant Rocket Motors", *Astronautica Acta*, *12* (4), 245–257 (1966).
(16) M. A. Karabeyoglu, D. Altman, and D. Bershader, "Transient Combustion in Hybrid Rockets", *AIAA paper* 95–2691, 1995.
(17) M. Kumar and K. K. Kuo, "Flame Spreading and Overall Ignition Transient", in K. K. Kuo and M. Summerfield (eds.), "Fundamentals of Solid Propellant Combustion", *Progress in Aeronautics and Astronautics*, *Vol. 90*, AIAA, New York 1984, pp. 305–360.
(18) D. R. Cruise, "*Theoretical Computation of Equilibrium Composition, Thermodynamic Properties, and Performance Characteristics of Propellant Systems (PEP Code)*", (1979), Naval Weapons Center, China Lake, CA, USA.
(19) S. DeSoto and H. A. Friedman, "Flame Spreading and Ignition Transients in Solid Grain Propellants", *AIAA J.*, *3* (3), 405–412 (1965).
(20) L. Strand, M. D. Johns, and R. L. Ray, "Characterization of Hybrid Rocket Internal Heat Flux and HTPB Fuel Pyrolysis", *AIAA paper* 94–2876, 1994.
(21) J. M. Lenoir and G. Robillard, "A Mathematical Method to Predict the Effects of Erosive Burning in Solid Propellant Rockets", *6th Symposium (International) on Combustion*. The Combustion Institute, Pittsburgh, Pennsylvania, 1957, pp. 663–667.

Symbols and Abbreviations

A	cross section area
a	speed of sound in liquid oxidizer
a_b	factor in burning rate law
a_i	extraneous equation parameters
C_D	discharge coefficient
C_R	coefficient of resistance
c_p	constant pressure specific heat
c_v	constant volume specific heat
D_i	extraneous equation parameters
e	stagnation energy
F_i	function
G	mass flux
h_c	enthalpy
h	heat transfer coefficient
K_g	gaseous products mass fraction in total propellant combustion products
k	thermal conductivity
k_b	erosive burning constant
L	propellant grain length
ℓ	oxidizer pipe line length
M	molecular weight
MR	mixture ratio

m mass
$\dot{m}$ mass flow rate
n burning rate exponent
p pressure
p^* extinguishing pressure limit
Pr Prandtl number
Q_i non-homogeneous terms
q rate of heat transfer
R gas constant
Re Reynolds number
$\dot{r}_b$ non-erosive burning rate
$\dot{r}_e$ erosive burning rate
S grain bore perimeter
T temperature
T_f propellant adiabatic flame temperature
t time
u gas velocity
v liquid oxidizer flow velocity
V volume
X_i molar fraction
x flow direction coordinate
Y_i mass fraction
y liquid oxidizer flow direction coordinate
z coordinate into the propellant grain
z_o penetration distance

Greek

α function
α_p thermal diffusivity
β erosive burning empirical constant
γ specific heat ratio
ε absorptivity
ζ_i coefficients
θ_k coefficients
λ_J eigenvalue
μ gas viscosity
ρ density
σ Stephan-Boltzmann constant
τ time delay
ϕ_i variable properties
χ function coefficient

Subscript

ac aft-end cavity
c combustion chamber
ch choked
eff effective
g gaseous phase products
hc head-end cavity
i,j,k,n indices
inj injector
ign igniter
m oxidizer manifold
o initial value
ox oxidizer
p propellant
part particle
pl pipe-line
s solid phase propellant combustion products
th nozzle throat
v valve

Acknowledgement

This research was supported by the Fund for the Promotion of Research at the Technion.

(Received April 19, 2000; Ms 2000/015)